Soils and Foundations 2016;56(4):593–607

HOSTED BY

ELSEVIER

The Japanese Geotechnical Society

Soils and Foundations

www.sciencedirect.com
journal homepage: www.elsevier.com/locate/sandf

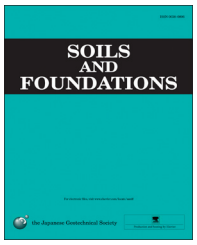

Technical Paper

A study of wave velocities and poisson ratio of recycled concrete aggregate

H. He, K. Senetakis*

University of New South Wales (UNSW), Sydney, Australia

Received 30 September 2015; received in revised form 3 March 2016; accepted 10 March 2016
Available online 2 August 2016

Abstract

The dynamic properties of two uniform recycled concrete aggregates (RCA) were investigated with a focus on shear wave velocities (V_s), primary wave velocities (V_p) and Poisson ratio (ν). The geotechnical characterization of these materials, one RCA with a fraction of 1.18–2.36 mm and the other with a fraction of 0.60–1.18 mm, was implemented through the quantification of particle shape descriptors, monotonic drained triaxial tests and one-dimensional compression tests. The grain damage of the RCA was quantified by examining the grading curves of the samples before and after the performance of the one-dimensional compression tests. Bender and extender element tests were carried out on dry samples under isotropic conditions of the confining pressure in order to investigate the dynamic properties of the RCA and comparisons were implemented between bender/extender elements and resonant column tests in torsional and flexural modes. The laboratory test results indicated that during the isotropic compression of the samples, V_s showed slightly higher sensitivity to pressure than V_p and the Poisson ratio was found to be dependent on pressure. However, during the isotropic unloading stage, V_s and V_p showed similar sensitivity to pressure and the Poisson ratio was found almost to be independent of pressure change. An empirical-type model proposed in the literature for crushed rock of irregular-shaped grains predicted within satisfactory limits the small-strain shear modulus of the RCA. The small-strain material damping in shear and the strain-dependent modulus and material damping were investigated and are discussed for a limited number of tests.

1. Introduction

The recycling and reuse of waste and demolition materials in civil engineering projects have received great attention in recent years due to environmental concerns and the pressure for these products to be utilized in efficient and cost-effective ways. The utilization of demolition materials, and related research on this areas, is more mature in the discipline of structural engineering than in geotechnical engineering; recycled concrete aggregate, for example, is reused in the production of new concrete. In recent years, geotechnical engineers have come to realize the potential for the application of industrial byproducts, waste and demolition materials in geotechnical projects (e.g. Gomes Correia et al., 2012; Soleimanbeigi et al., 2012; Warner and Edil, 2012). While the available literature investigating the geotechnical properties of for recycled concrete aggregate (RCA) is relatively limited, most research work has indicated promising applications for RCA in particular. Previous research on the geotechnical properties of RCA have focused, primarily, on its physical properties and its static behavior as well as other properties associated with pavement engineering applications (e.g. Chini et al., 2001; Sivakumar et al., 2004; Poon and Chan, 2006a, 2006b; Tam and Tam, 2007; Arulrajah et al., 2013; Bhuiyan et al., 2015 among others).

As is the case with all granular materials, the complete geotechnical characterization of RCA requires experiments using dynamic test methods, for example resonant column (Richart et al., 1970; Ishihara, 1996) or bender element tests

*Corresponding author.
E-mail address: k.senetakis@unsw.edu.au (K. Senetakis).
Peer review under responsibility of The Japanese Geotechnical Society.

http://dx.doi.org/10.1016/j.sandf.2016.07.002

(Shirley and Anderson, 1975). These methods allow the elastic and attenuation properties to be captured: these are essential in geotechnical engineering and to the seismic design of civil engineering facilities. In the present study, a preliminary investigation of the dynamic properties of recycled concrete aggregate was conducted on two uniform fractions using advanced dynamic test methods. The geotechnical characterization of the RCA was based on conventional laboratory tests, including the determination of the specific gravity of solids, particle shape quantification, one-dimensional compression tests and consolidated drained monotonic triaxial tests.

2. Materials and methods

2.1. Materials used and experimental methods for basic geotechnical characterization

The recycled concrete aggregate (RCA) used in the study was provided by a local supplier from New South Wales, Australia. The material was sieved and two uniform fractions, denoted as RCA04 (fraction 0.60–1.18 mm) and RCA05 (fraction 1.18–2.36 mm), were studied in the laboratory. The grain size characteristics of the RCA fractions are given in Table 1. An image of the fraction RCA05 is provided in Fig. 1.

Conventional laboratory tests and procedures were used in the geotechnical characterization of the RCA. The specific gravity of solids (G_s) was found equal to 2.47 for both the RCA fractions. The shape of the particles was quantified based on the visual observation of a representative number of grains from each fraction through an optical microscope and the use of an empirical chart proposed by Krumbein and Sloss (1963). From each fraction, twenty five grains were randomly chosen and two operators quantified the particle shape by means of two descriptors; particle sphericity (S) and particle roundness (R). It was found that the RCA fractions had grains of low roundness, but relatively medium to high sphericity. The mean value and the standard deviation for the descriptors S and R are summarized in Table 1. It has been reported that particle shape controls the packing as well as the mechanical and dynamic behavior of granular materials (e.g., Cho et al., 2006; Senetakis et al., 2012; Payan et al., 2016). Cho et al. (2006) introduced a third particle shape descriptor, namely the regularity, which is the arithmetic mean of S and R. The regularity effectively captures, in quantitative terms, the effects of both S and R on the mechanical behavior of granular soils. For the RCA04 and RCA05, the mean value of the regularity descriptor was found equal to 0.50 and 0.49, respectively; that is, the grains of the RCA fractions were relatively irregular in shape.

Table 1
Recycled concrete aggregate (RCA) fractions used in the study.

Code of sample	RCA04	RCA05
Fraction (mm)	0.60–1.18	1.18–2.36
Specific gravity G_s	2.47	2.47
Mean grain size D_{50} (mm)	0.84	1.67
Coefficient of uniformity C_u	1.40	1.30
Coefficient of curvature C_c	0.90	0.97
Sphericity S (mean)	0.71	0.67
Sphericity standard deviation	0.15	0.21
Roundness R (mean)	0.29	0.31
Roundness standard deviation	0.13	0.16
Regularity	0.50	0.49
Regularity standard deviation	0.13	0.15
Critical state parameter λ	0.21	–
Critical state parameter Γ	2.56	–
Angle of shear strength at critical state (deg)	31	–

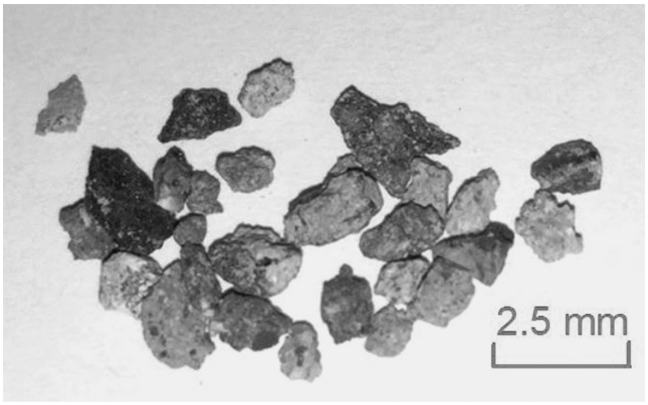

Fig. 1. Image of the recycled concrete aggregate fraction RCA05 (1.18–2.36 mm).

Apart from the quantification of the specific gravity and shape of particles, one-dimensional (oedometer) tests were performed on dry samples for both the RCA04 and RCA05 fractions, prepared at variable initial densities for the study of the compression behavior. Because the aim of the oedometer tests for this study was solely to investigate the grain damage for the RCA, the application of relatively high pressures was required. Consolidated drained (CD) monotonic triaxial tests were performed on fully saturated samples for the RCA04 fraction for a preliminary investigation of the angle of shear strength at peak and critical states. The one-dimensional compression test samples and the triaxial test samples are summarized in Tables 2 and 3, respectively. After the completion of the oedometer tests, the grading curves of the samples were examined through a series of sieves and the particle breakage was quantified adopting a simple method proposed by Hardin (1985) for measuring what is called Relative Breakage (Br). Note that the oedometer tests were performed for a range of maximum vertical stresses from about 1.0 MPa to 3.9 MPa in order to capture the compression behavior of the samples in the range of small to relatively high pressures with measurable grain damage, whereas the triaxial tests were carried out at relatively small to medium isotropic consolidation pressures ranging from 100 to 500 kPa. The oedometer test samples were of about 20 mm in thickness and 50 or 75 mm in diameter and the triaxial test samples were of about 100 mm in height and 50 mm in diameter. Because of the small size of the oedometer samples, the initial specific volume was evaluated based on two independent methods similarly to the procedures described by Altuhafi and Coop (2011) and Rocchi and Coop (2014) considering that the samples were prepared and tested in a dry state. The first

Table 2
One-dimensional compression tests on dry samples for the geotechnical characterization of the recycled concrete aggregate.

No.	Specimen code	Preparation method	γ_{do} (kN/m^3)	ν_0	Δv_i	$\sigma'_{v,max}$ (MPa)	$\epsilon_{v,1}$ (%)	$\epsilon_{v,2}$ (%)	B_r (%)
(1)	(2)	(3)	(4)	(5)	(6)	(7)	(8)	(9)	(10)
1	RCA04-OED1	Compaction	11.45	2.117	0.113	1.10	8.7	7.8	1.9
2	RCA04-OED2	Compaction	11.27	2.151	0.035	1.10	9.0	8.0	2.5
3	RCA04-OED3	Hand-spooning	10.98	2.207	0.012	2.44	15.0	13.1	4.3
4	RCA04-OED4	Compaction	11.26	2.152	0.039	3.85	18.1	16.2	7.0
5	RCA04-OED5	Compaction	12.57	1.928	0.008	0.98	7.7	6.9	1.7
6	RCA04-OED6	Compaction	12.31	1.969	0.020	3.85	15.1	12.6	4.1
7	RCA05-OED1	Hand-spooning	10.87	2.230	0.004	0.98	10.7	9.4	2.0
8	RCA05-OED2	Hand-spooning	10.47	2.315	0.012	2.44	18.7	17.0	5.5
9	RCA05-OED3	Compaction	11.77	2.059	0.012	0.98	7.6	6.5	1.3
10	RCA05-OED4	Compaction	11.88	2.039	0.036	1.10	7.9	6.9	1.8
11	RCA05-OED5	Compaction	11.80	2.053	0.031	2.44	13.8	12.0	3.5

No1–No6: fraction RCA04 0.60–1.18 mm, No7–No11: fraction RCA05 1.18–2.36 mm,
(3) compaction was applied for dense and hand-spooning was applied for relatively loose samples (4)(5) initial unit weight and specific volume at a zero vertical stress,
(6) difference in initial specific volume measured from two independent methods (described in Altuhafi and Coop, 2011) (7) maximum applied vertical stress (8) volumetric strain at $\sigma'_{v,max}$,
(9) volumetric strain at zero vertical stress after the completion of the unloading stage,
(10) relative breakage based on Hardin (1985) definition.

Table 3
CD monotonic triaxial tests on fully saturated samples for the geotechnical characterization of the recycled concrete aggregate.

No.	Specimen code	Preparation method	$\gamma_{do(c)}$ (kN/m^3)	$\nu_{0(c)}$	$w_{0(c)}$ (%)	p'_0 (kPa)	ξ	ϕ'_p (deg)
(1)	(2)	(3)	(4)	(5)	(6)	(7)	(8)	(9)
1	RCA04-TR1	Compaction	12.06	2.009	40.85	100	−0.584	43
2	RCA04-TR2	Compaction	10.54	2.299	52.59	100	−0.294	34
3	RCA04-TR3	Compaction	11.90	2.037	41.98	300	−0.325	37
4	RCA04-TR4	Compaction	11.83	2.049	42.47	500	−0.206	32

(4)(5)(6) Initial unit weight, specific volume and water content after the completion of the consolidation stage before the shearing stage (7) consolidation pressure before the shearing stage.
(8) State parameter, expresses the state of the soil before the shearing stage.
(9) Angle of shear strength at peak state.

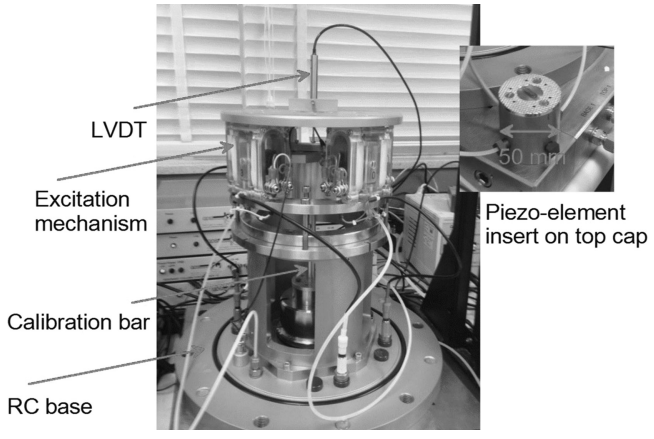

Fig. 2. Resonant column of fixed-free ends used in the study and close-up view of top cap with piezo-element insert.

method was based on the measurement of the initial thickness of the sample and its known diameter, while the second method was based on the final thickness of the sample after the completion of the unloading stage and the total settlement, which settlement was recorded during the experiment with a dial gauge. For the representation of the specific volume - vertical stress curves, an average specific volume value calculated from the two methods is used in the study. The difference in specific volume, denoted as Δv_i, between the two methods used to estimate the oedometer sample specific volume is provided in Table 2 for each specimen.

2.2. Dynamic testing program

Seven samples from the RCA04 fraction and five samples from the RCA05 fraction were prepared in a resonant column apparatus of fixed-free ends with embedded piezo-element (bender/extender element) inserts and tested in a dry state under isotropic pressures in a range of 25 kPa to 800 kPa. The resonant column used in the study is a computer-controlled apparatus supplied from GDS Instruments, UK. An image of the apparatus and a close-up view of the top cap with a piezo-element insert are given in Fig. 2. The drive mechanism

attached to the top of the sample was composed of four coils and four magnets. The system is capable of subjecting the sample to both torsional and flexural modes of vibration, allowing for independent measurements of shear and Young's moduli to be conducted simultaneously. Calibrations of the resonant column apparatus were carefully carried out following the ASTM D4015-92 specifications (ASTM, 1992), the recommendations by Cascante et al. (1998) and Kumar and Madhusudhan (2010a) with regard to the flexural mode of vibration and the experience of the authors. The bender/extender element inserts used in the study were comprised of piezoelectric ceramic bi-morphs (Kumar and Madhusudhan, 2010b). Because of their configuration, it was possible to propagate both primary (P) and shear (S) waves and therefore, to measure the Poisson's ratio. The piezo-elements are connected in two different configurations (Kumar and Madhusudhan, 2012b, 2010c); the top of the sample is embedded with the P-wave receiver and S-wave source, and the bottom of the sample is embedded with the P-wave source and S-wave receiver. In measuring P-waves, the extender element configuration is used and in conducting S-waves measurements, the bender element configuration is used. The alteration of the system, i.e. extender or bender element tests, is implemented through the software that controls the experiments, supplied from GDS Instruments. Discussion on the interpretation of the bender elements in measuring shear wave velocities and shear moduli and the signal analysis for the time arrival estimation may be found in Jovicic et al. (1996), Leong et al. (2005), Lee and Santamarina (2005), Ogino et al. (2015) and Gu et al. (2015), among others. Discussion on the measurement of the time arrival for the estimation of the primary wave velocities and the performance of the extender elements may be found in Kumar and Madhusudhan (2010b, 2010c) or Leong et al. (2009).

The samples were prepared at variable initial densities in a dry state in a plastic split mold with an internal diameter of about 50 mm and a height of about 100 mm. Dense samples were prepared in layers and each layer was densified by manually applying vibration with a thin plastic rod with rounded edges. For medium dense to relatively loose samples, the air-pluviation method was adopted. After the samples were prepared and before the set of resonant column tests began, including the placement of the drive mechanism, the magnets and the triaxial cell, a small vacuum of about 5 kPa was applied in order to support the specimen. The vacuum was gradually removed during the application of the first level of isotropic confining pressure (p') equal to 25 kPa or 50 kPa.

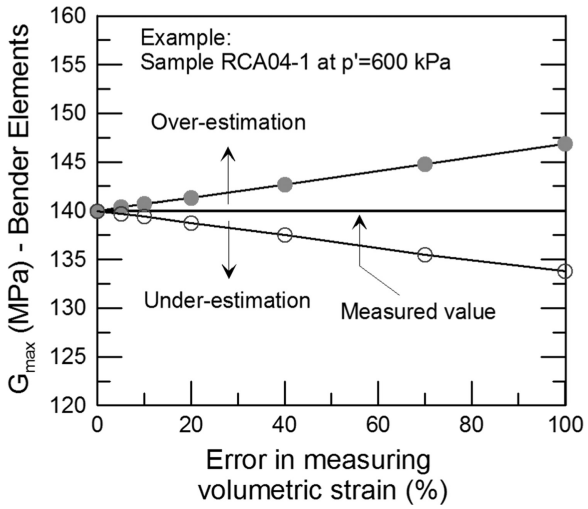

Fig. 3. Example showing the sensitivity of small-strain shear modulus to an error in measuring the volumetric strain (Note: The volumetric strain for dry samples is estimated in the study based on the measurement of the axial strain and the assumption of isotropic compression).

Table 4
Dynamic testing program on dry samples.

No.	Specimen code	Preparation method	γ_{d0} (kN/m^3)	ν_0	n_0 (%)	Small-strain measurements	Medium-strain measurements
(1)	(2)	(3)	(4)	(5)	(6)	(7)	(8)
1	RCA04-1	Air-pluviation	10.70	2.264	55.83	BE - TOR - FLEX - FVD	–
2	RCA04-2	Compaction	11.14	2.175	54.02	BE - TOR - FLEX - FVD	–
3	RCA04-3	Compaction	11.34	2.136	53.18	BE - TOR - FLEX	–
4	RCA04-4	Compaction	11.16	2.171	53.94	BE - TOR	TOR:100,400
5	RCA04-5	Air-pluviation	10.82	2.240	55.36	TOR	–
6	RCA04-6	Compaction	11.51	2.106	52.52	TOR	–
7	RCA04-7	Compaction	11.69	2.073	51.76	TOR - FVD	–
8	RCA05-1	Compaction	10.85	2.233	55.22	BE - TOR - FLEX - FVD	–
9	RCA05-2	Compaction	11.01	2.200	54.55	BE - TOR - FLEX - FVD	TOR: 200
10	RCA05-3	Compaction	10.78	2.248	55.52	BE - TOR - FLEX - FVD	–
11	RCA05-4	Compaction	11.15	2.173	53.98	BE – TOR	TOR:200
12	RCA05-5	Compaction	11.10	2.183	54.19	BE - TOR - FLEX	TOR: 100,400

No1–No7: fraction RCA04: 0.60–1.18 mm, No8–No12: fraction RCA05 1.18–2.36 mm,
(3) compaction was applied for dense and air-pluviation was applied for relatively loose samples.
(4)(5)(6) Initial unit weight, specific volume and porosity measured at a vacuum of 5 kPa.
BE: Bender/extender element tests for S-wave and P-wave velocities measurements.
TOR: Torsional resonant column tests for shear modulus measurements.
FLEX: Flexural resonant column tests for Young's modulus measurements.
FVD: Measurements of small-strain damping using the free-vibration decay method.
Medium-strain measurements: Torsional resonant column tests, 100 200 and 400 denote p' in kPa.

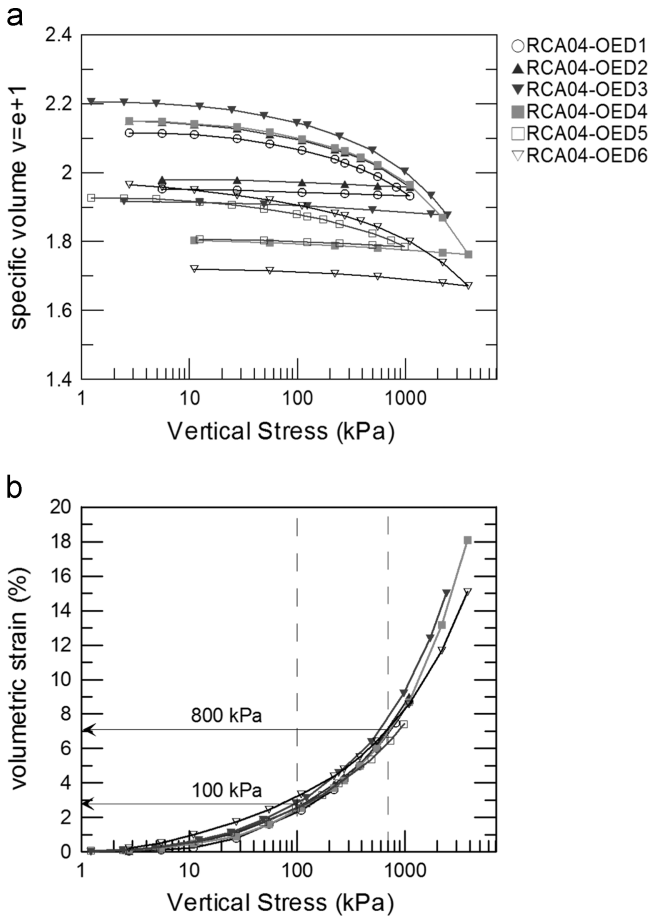

Fig. 4. One-dimensional compression test results for the RCA04 fraction: (a) specific volume - vertical stress during loading-unloading and (b) volumetric strain - vertical stress during loading.

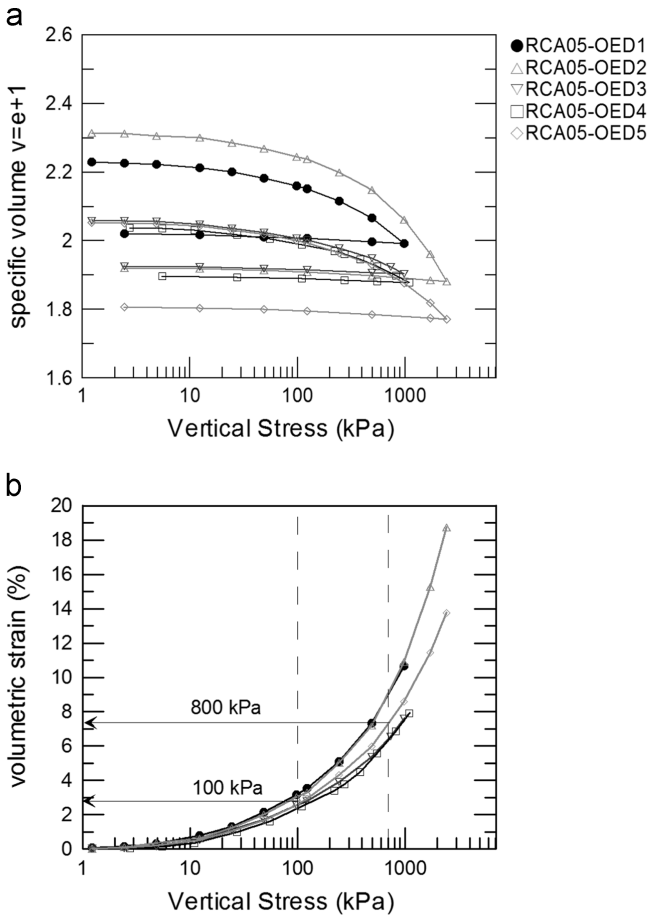

Fig. 5. One-dimensional compression test results for the RCA05 fraction: (a) specific volume - vertical stress during loading-unloading and (b) volumetric strain - vertical stress during loading.

Measurements of sample volume were conducted carefully with a calliper while the specimen was supported by the vacuum in order to estimate the initial specific volume ($\nu_0 = e_0 + 1$), where e_0 is the initial void ratio. A vertically positioned linearly variable differential transformer (LVDT) attached to top of the sample with a precision of 0.001 mm was used to record changes in sample height.

After the application of the maximum isotropic pressure of 800 kPa, most samples were subjected to isotropic swelling (unloading of p'). At each step of p' increase or decrease, the shear wave velocities (V_s) and primary wave velocities (V_p) were measured through the bender and extender element tests, respectively. V_s was also measured based on small-strain torsional resonant column tests in order to compare the different methods in measuring small-strain stiffness and validate the interpretation of the time arrival from the bender element tests. For a limited number of samples, flexural resonant column tests were conducted to estimate the Young's modulus as well as measurements of stiffness and damping from small to medium strain amplitudes. In Table 4, the dynamic testing program is summarized with associated information regarding the sample preparation method, the initial unit weight (γ_{d0}), specific volume (ν_0) and porosity (n_0) of the samples and the mode of the dynamic tests.

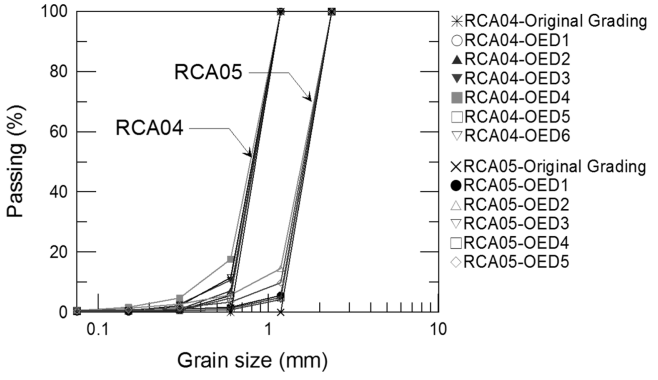

Fig. 6. Alteration of grading curves of the samples after the completion of the one-dimensional compression tests due to particle breakage.

During the isotropic compression of the RCA samples, the maximum volumetric strain was in the order of 5%–8% at $p' = 800$ kPa. During the unloading stage, it was revealed that most of this deformation was plastic in nature. Note that the volumetric strain (ϵ_v) of the samples was derived based on the measured axial strain (ϵ_a) from the vertically positioned LVDT attached to the top of the sample and the assumption of isotropic compression, thus ϵ_v equals three times ϵ_a. This is because the resonant column samples were tested in a dry

state, rendering it technically impossible to measure the volume changes of the samples in a straightforward way. However, the volumetric strain measured on fully saturated samples during the consolidation stage in the triaxial apparatus (samples are summarized in Table 3) was very similar to the volumetric strain estimated in the resonant column samples (samples summarized in Table 4) based on the previously mentioned assumptions. For the triaxial samples, because they were consolidated in a fully saturated state, the volumetric strain was measured in a straightforward way from the measurement of the changes of sample pore water volume with a volume controller-regulator.

However, the overall uncertainties or introduced errors in estimating the volumetric strain of the dry sample, and thus the changes in density and void ratio, did not have an important effect on the resultant soil modulus. In Fig. 3, an example of the sensitivity of G_{max} to a possible error in measuring the volumetric strain for the dry samples is illustrated. This example corresponded to the sample RCA04-1 at $p'=600$ kPa. The figure illustrates that if the error in the estimated volumetric strain is 100%, which is an extreme case in daily practice, the resultant error in the measured G_{max} will be no more than 3% to 4%. Note that because of relatively small to medium compressibility of the RCA samples, very small changes were noted in the volume of the sample during the elevation of the confining pressure for the particular range of stresses applied in the resonant column. This was also verified by the check of the sample volume changes of the fully saturated samples in the triaxial tests.

3. Results and discussion

3.1. Brief discussion on the oedometer and triaxial test results and grain damage

The one-dimensional compression test results by means of specific volume - vertical stress ($\nu-\sigma'_v$) during the loading and unloading stages are summarized in Figs. 4(a) and 5(a). The volumetric strain against the vertical stress curves ($\epsilon_v-\sigma'_v$) during the loading process are summarized in Figs. 4(b) and 5 (b) and at representative stresses (100 and 800 kPa), typical values of the volumetric compression of the samples are depicted. The volumetric strain (ϵ_{v1}) that corresponded to the maximum applied vertical stress ($\sigma'_{v,max}$) ranged from about 8% to about 18% depending on the level of $\sigma'_{v,max}$ and the initial density of the samples; for a given $\sigma'_{v,max}$, looser samples compressed more, resulting in greater ϵ_{v1} values than denser samples. Most of the deformation during the loading stage was plastic in nature, providing almost horizontal curves in the $\nu-\sigma'_v$ plane during unloading. The values of the volumetric strain at the maximum applied vertical stress (ϵ_{v1}) and the volumetric strain after the completion of the unloading stage, denoted as ϵ_{v2}, are summarized in Table 2.

The breakage of grains for the RCA04 and the RCA05 was quantified and the relative breakage (B_r) values of the samples are summarized in Table 2. The final grading curves of the samples subjected to the one-dimensional compression tests are summarized in Fig. 6. Note that the alteration of the final grading in comparison to the initial grading of the samples was slightly more pronounced for higher applied maximum vertical stresses. The values of B_r were equal to or less than 2.5% for samples subjected to a maximum vertical stress of about 1.0 MPa, indicating almost negligible grain damage for stresses up to 1.0 MPa. This was verified by additional 1-dimensional compression tests that were conducted by the authors at stresses below 1 MPa, as well as the resonant column tests, which were conducted at a maximum isotropic pressure of 800 kPa. No measurable grain damage or alteration of the initial grading curves of the samples was noted in these tests. The relative breakage did not exceed values of about 5.5% to 7.0% for samples subjected to a maximum vertical stress of approximately 2.5 to 3.9 MPa. For the limited number of the oedometer tests conducted in the study and for a given maximum applied vertical stress, a slight increase of B_r for looser samples was observed, which is in agreement with the findings by Altuhafi and Coop (2011). However, because of the limited number of the one-dimensional compression experiments, no firm conclusions can be drawn and further investigation is necessary. It should also be noted that for the range of pressures in the study, the complete convergence of the compression curves for both fractions to a unique limiting line was not observed. To achieve convergence, much greater pressures may be required. However, this was beyond the scope of the present work.

In the literature, complementary laboratory studies investigating the compression behavior of sands, the grain damage in granular soils and the role of grain damage in the mechanics of soils may be found in Nakata et al. (2001), Altuhafi and Coop (2011), Shipton and Coop (2012), Vilhar et al. (2013), or Ghafghazi et al. (2014). The oedometer test results with quantification of grain damage indicated that for the range of pressures considered in the study, the relative breakage for the RCA samples was slightly greater than the corresponding breakage observed in quartz sands, with almost negligible

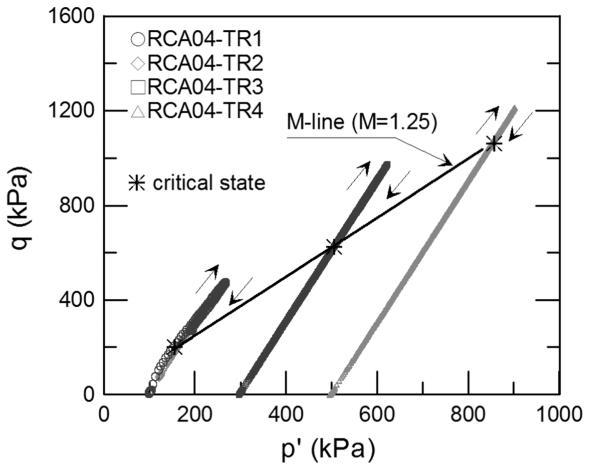

Fig. 7. CD monotonic triaxial test results on fully saturated samples for the fraction RCA04: Representation in the deviatoric stress - confining pressure plane.

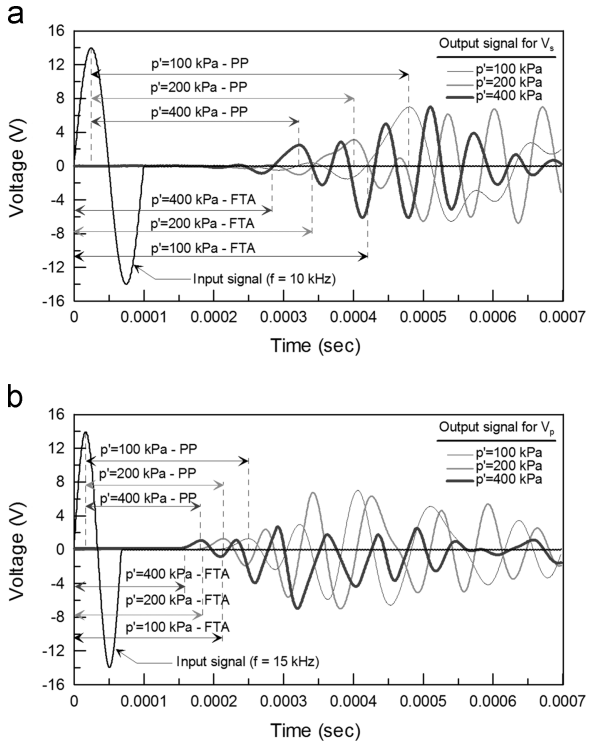

Fig. 8. Example of the interpretation and the signal processing for the bender/extender element tests against (a) shear waves (V_s) propagation and (b) primary waves (V_p) propagation for sample RCA05-4: PP denotes peak-to-peak time arrival and FTA denotes first time arrival.

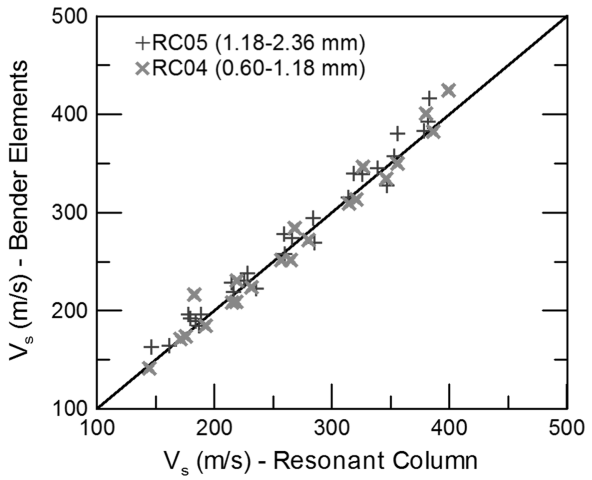

Fig. 9. Comparison of the measured shear wave velocities between the bender element tests and the torsional resonant column tests.

grain damage to soils for this range of stresses. However, the computed B_r for the RCA samples was lower than the B_r values reported in the literature for sands with highly crushable grains, for example carbonate sands, which are characterized be relative breakage values in excess of 10% or 15% for this range of pressures, i.e. between 1 and 4 MPa.

The CD monotonic triaxial test results are summarized in Fig. 7 in terms of deviatoric stress - confining stress plots (q–p'). Since the results in Fig. 7 indicate a value of M equal to 1.25, based on the well-known expression of Eq. (1) found in

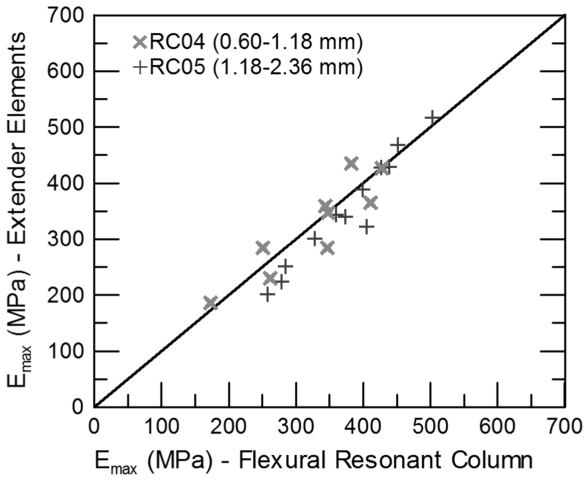

Fig. 10. Comparison of the measured small-strain Young's modulus between the extender element tests and the flexural resonant column tests.

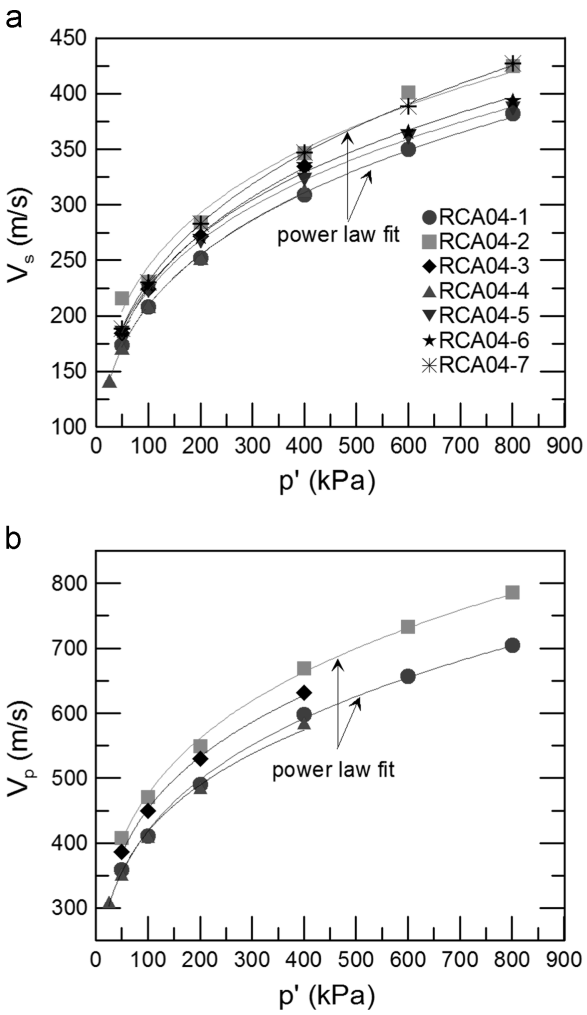

Fig. 11. Bender/extender element test results for the fraction RCA04: (a) V_s–p' and (b) V_p–p' relationships during isotropic compression and corresponding fitting curves of a power-law type (Note: for samples RCA04-5, RCA04-6, RCA04-7 only resonant column tests were performed).

any Soil Mechanics textbook, the angle of shear strength at the critical state was equal to about 31 degrees. In Eq. (1), ϕ'_{cv} denotes the angle of shear strength at the critical state (or constant

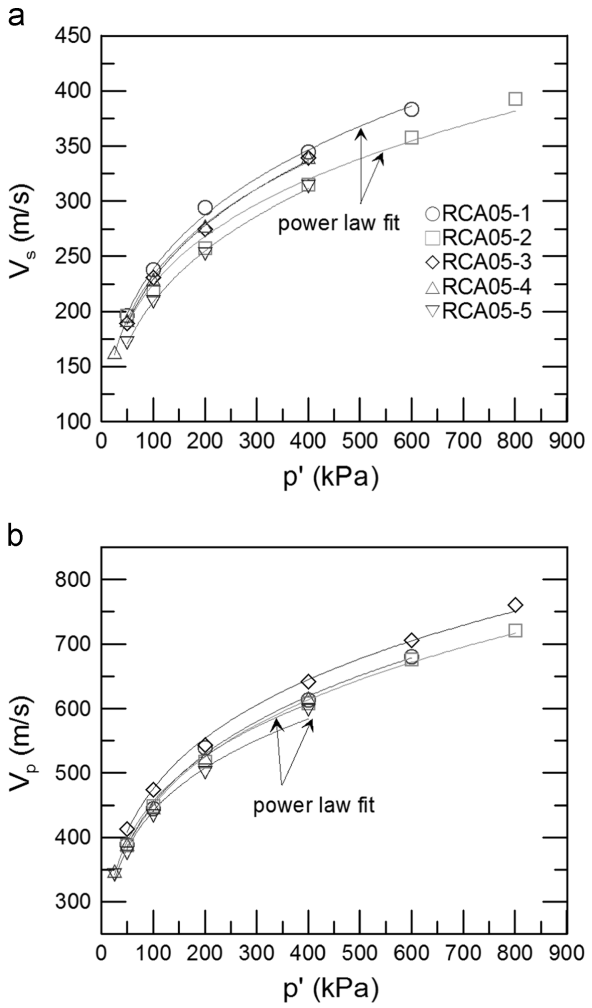

Fig. 12. Bender/extender element test results for the fraction RCA05: (a) V_s–p' and (b) V_p–p' relationships during isotropic compression and corresponding fitting curves of a power-law type.

volume).

$$M = \frac{6 \times \sin(\phi_{cv}')}{3 - \sin(\phi_{cv}')} \quad (1)$$

In Table 3, the values of the angle of shear strength of the samples at a peak state are summarized (denoted as ϕ'_p) as well as the initial state of the samples after the completion of the consolidation stage and before the shearing with respect to the critical state line, which was expressed through the state parameter, ξ (after Been, Jefferies, 1985). The state parameter is given in Eq. (2). In this formula, ν and e denote specific volume and void ratios, respectively, and v_{cv} and e_{cv} denote the specific volume and void ratio at the critical state, respectively. ξ denotes the vertical distance between the current state of the sample and the critical in the specific volume–pressure plane. Based on the critical state soil mechanics theory, negative values of the state parameter indicate that the sample is on the dry side of the critical state line

$$\xi = v - v_{cv} = e - e_{cv} \quad (2)$$

For the set of triaxial test samples included in the study, ϕ'_p ranged from 32 to 43 degrees depending on the level of p'_0 and the initial state of the samples with respect to the critical state line. The critical state parameters λ and Γ for the RCA04 were found equal to 0.21 and 2.56, respectively (summarized in Table 1). These values corresponded to the void ratio - confining pressure plane, i.e. Γ denotes the void ratio at $p'=1$ kPa.

3.2. The performance of the samples in bender/extender element and torsional/flexural resonant column tests

In the study, shear wave velocities and shear moduli were measured through bender element tests. The validation of the

Table 5
Elastic constants of specimens during dynamic element tests under. isotropic compression (increasing p').

No.	Specimen code	ν_0	V_s constants		V_p constants		ν constants	
			a_s	b_s	a_p	b_p	a_v	b_v
(1)	(2)	(3)	(4)	(5)	(6)	(7)	(8)	(9)
1	RCA04-1	2.264	56.2	0.29	132.2	0.25	0.43	−0.05
2	RCA04-2	2.175	73.7	0.26	156.8	0.24	0.37	−0.03
3	RCA04-3	2.136	60.4	0.29	152.4	0.24	0.46	−0.07
4	RCA04-4	2.171	56.2	0.29	144.5	0.23	0.46	−0.07
5	RCA04-5	2.240	65.0	0.27	–	–	–	–
6	RCA04-6	2.106	65.1	0.27	–	–	–	–
7	RCA04-7	2.073	59.6	0.29	–	–	–	–
8	RCA05-1	2.233	69.0	0.27	158.9	0.23	0.45	−0.08
9	RCA05-2	2.200	69.3	0.26	159.6	0.23	0.42	−0.05
10	RCA05-3	2.248	62.3	0.28	172.5	0.22	0.52	−0.09
11	RCA05-4	2.173	68.4	0.27	175.1	0.21	0.48	−0.09
12	RCA05-5	2.183	70.6	0.25	172.9	0.20	0.46	−0.08

(3) Initial specific volume ($\nu_0 = e_0 + 1$) at a vacuum of 5 kPa
(4) (5) Shear wave velocity–pressure constants
(6) (7) Primary wave velocity–pressure constants
(8) (9) Poisson ratio–pressure constants

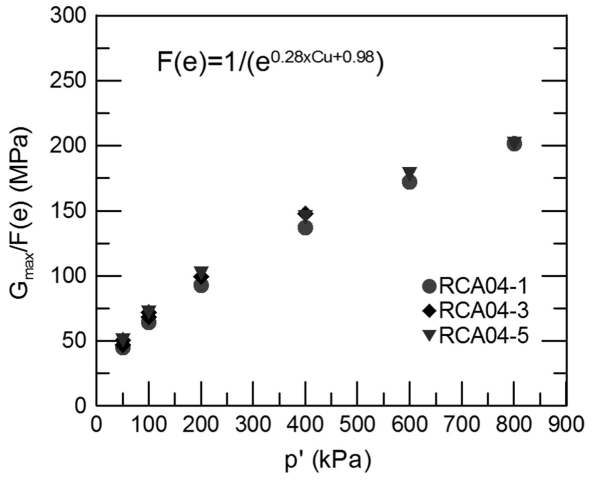

Fig. 13. Small-strain shear modulus normalized with respect to a void ratio function proposed in the literature (Senetakis et al., 2012) against the confining pressure during isotropic compression: Representative results for the fraction RCA04.

bender element test signal analysis was implemented through additional torsional resonant column tests. In particular, since the mass density of the sample (ρ) and the resultant shear modulus $G_{\max}$, V_s from the resonant column tests were derived using Eq. (3), comparisons could be made between the bender element and torsional resonant column tests.

$$G_{max} = \rho \times V_s^2 \tag{3}$$

Primary wave velocities (V_p) were measured in a straightforward way from the extender element tests. For a limited number of tests, flexural resonant column tests were conducted and an analysis of the results was carried out by adopting the formulae presented by Cascante et al. (1998) for the computation of the Young's modulus, E_{max}. Based on the measured V_s and V_p, from the bender and extender element tests, the Poisson's ratio (ν) was derived from Eq. (4). Thus, from the known constrained modulus (M_{max}) and the formulae from the theory of elasticity, (Eqs. (4) to 6) were applied for the indirect computation of E_{max} from the extender elements, and comparisons could be made with the flexural resonant column test results.

$$v = \frac{0.5 \times V_P^2 - V_S^2}{V_P^2 - V_S^2} \tag{4}$$

$$M_{max} = \rho \times V_p^2 \tag{5}$$

$$E_{max} = \frac{M_{max} \times (1+\nu) \times (1 - 2 \times \nu)}{(1 - \nu)} \tag{6}$$

For a limited number of tests, the samples were subjected to small-strain material damping measurements using the free-vibration decay method (ASTM, 1992) and medium-strain torsional resonant column testing.

For the bender/extender element tests, the time arrival was estimated as an average value derived from the first-time arrival (FTA) and the peak-to-peak (PP) methods. Based on the

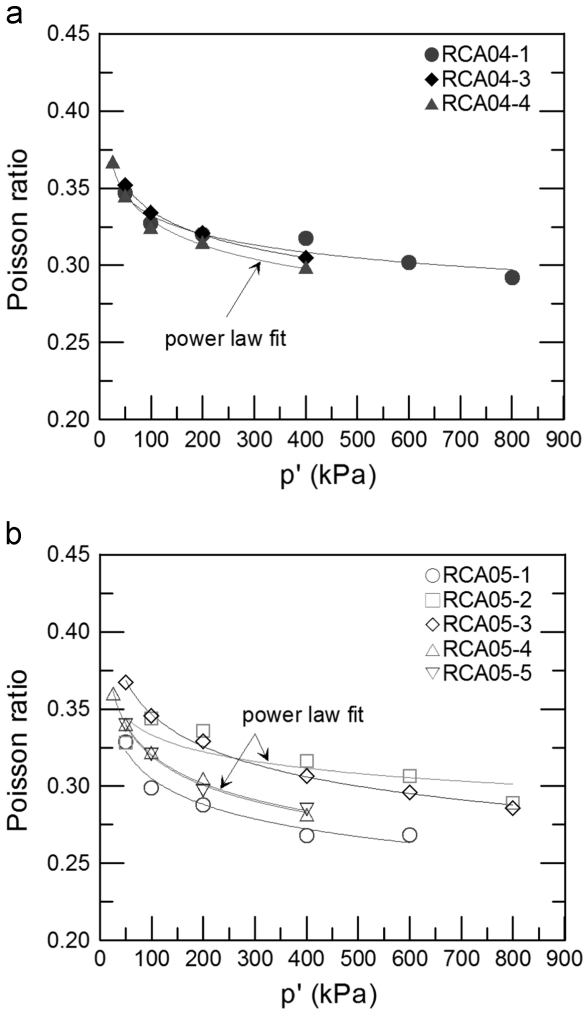

Fig. 14. Bender/extender element test results for the fraction (a) RCA05 and (b) RCA04: Poisson ratio against confining pressure during isotropic compression and corresponding fitting curves of a power-law type.

estimated time arrival and the vertical tip-to-tip distance of the piezo-element inserts, the wave velocity was computed. For V_s and V_p, a frequency of 10 kHz and 15 kHz was used, respectively, for the input sinusoidal signal which had an amplitude of 14 V. Typical plots of input and output signals against the time for sample RCA05-4 at p' equal to 100, 200 and 400 kPa are given in Fig. 8. In the same figure, an interpretation of the FTA and PP methods is provided. Note that in the measurements of S-wave and P-wave velocities, satisfactory agreement was achieved between the first-time and peak-to-peak time arrival methods. For most samples, the difference in the measured S-wave velocities was found within a range of 1% to 5% and the difference in the measured P-wave velocities was found within a range of 4% to 7% between the two methods for estimating time arrival. A comparison of V_s values derived from the bender elements, using an average value between the FTA and PP methods, and the torsional resonant column tests is provided in Fig. 9. The V_s values between the two methods converged satisfactorily. Note that in the following sections, the V_s–p' relationships and

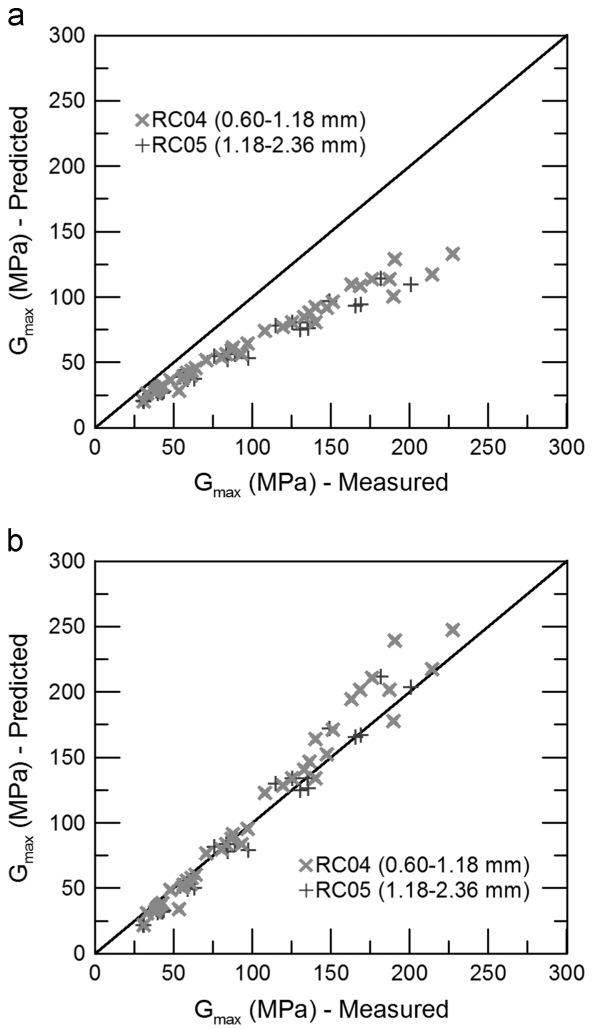

Fig. 15. Comparison between estimated and measured values of small-strain shear modulus for the RCA: The estimated values are computed based on a model proposed by Senetakis et al. (2012) for (a) river sand of relatively regular-shaped grains and (b) crushed rock of irregular-shaped grains.

Poisson's ratio derivations are based on bender element tests for all the samples, apart from samples RCA04-5, RCA04-6 and RCA04-7, for which bender element tests were not conducted and thus shear wave velocities were measured solely from the torsional resonant column tests. A comparison of Young's moduli between the extender element tests and the flexural resonant column tests is given in Fig. 10. Within the scatter of the data, the comparison was satisfactory.

3.3. V_s–p' and V_p–p' relationships during isotropic compression

Plots of shear wave velocity and primary wave velocity against the confining pressure for all the samples during the isotropic compression stage are given in Fig. 11 for the RCA04 and in Fig. 12 for the RCA05. The V_s–p' and V_p–p' relationships were fitted with power law type curves of the

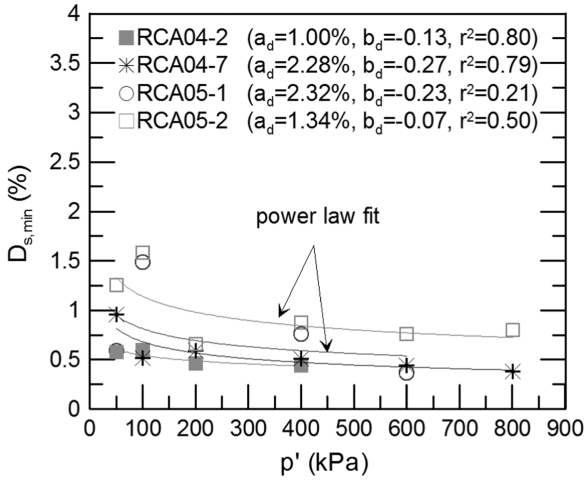

Fig. 16. Small-strain material damping against confining pressure during isotropic compression of the RCA samples and correspond fitting curves of a power law type (the constants of the fitting curves and the correlation coefficients r^2 are depicted in the figure).

general formula of (Eqs. (7) and 8):

$$V_s = a_s \times \left(p'\right)^{b_s} \tag{7}$$

$$V_p = a_p \times \left(p'\right)^{b_p} \tag{8}$$

In these equations, a_s, a_p, b_s and b_p are material constants which depend, primarily, on particle shape, size distribution and overall morphology (Santamarina and Cascante, 1998; Cho et al., 2006; Senetakis et al., 2012, 2016; Senetakis and Madhusudhan, 2015; Payan et al., 2016). The power b_s and the power b_p reflect the sensitivity of the wave velocity to pressure and the particle-to-particle contact response of geo-materials which is brittle to plastic in nature. Cha et al. (2014) have linked the constants of (Eqs. (7) and 8) to the compressibility C_c. On the other hand, the constants a_s, a_p also depend on the initial packing which is incorporated in many empirical-type models proposed in the literature (e.g. Hardin and Richart, 1963; Wichtmann, Triantafyllidis Th., 2009; Senetakis et al., 2012; Senetakis and Madhusudhan, 2015).

The analysis of the results led to the estimation of the constants a_s, a_p, b_s and b_p for all the samples during the isotropic compression stage. These values are summarized in Table 5. The power b_s had values in a range of 0.26 to 0.29 for the RCA04 and in a range from 0.25 to 0.28 for the RCA05. These values are in agreement with values reported in the literature for sands of irregular shaped grains, for example crushed rock. On the other hand, for sands of relatively rounded and regular in shape grains, the reported values of b_s in the literature range, typically, between 0.22 and 0.25 (e.g. Cho et al., 2006; Senetakis et al., 2012; Payan et al., 2016). Note that during the isotropic compression stage, the power b_p had lower values than b_s for all the samples. For the RCA04, b_p ranged from 0.23 to 0.25 and for the RCA05, b_p ranged from 0.20 to 0.23. These results implied that the sensitivity of V_s to pressure was greater than the sensitivity of V_p to pressure.

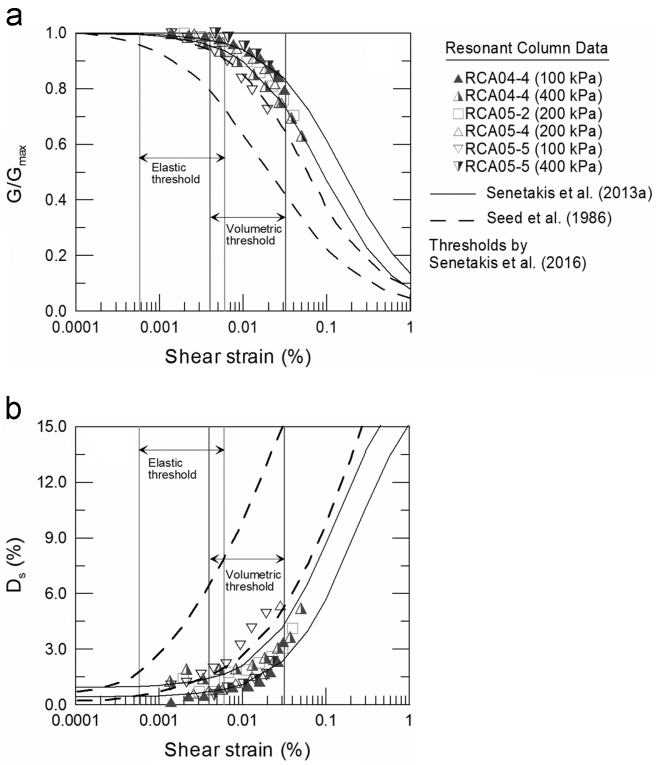

Fig. 17. Medium-strain resonant column test results: (a) normalized shear modulus degradation against shear strain and (b) material damping increase against shear strain and corresponding upper-lower bounds of curves proposed in the literature. (Note: a range for the elastic and volumetric threshold strains is also depicted in the figure based on the literature data on granular soils).

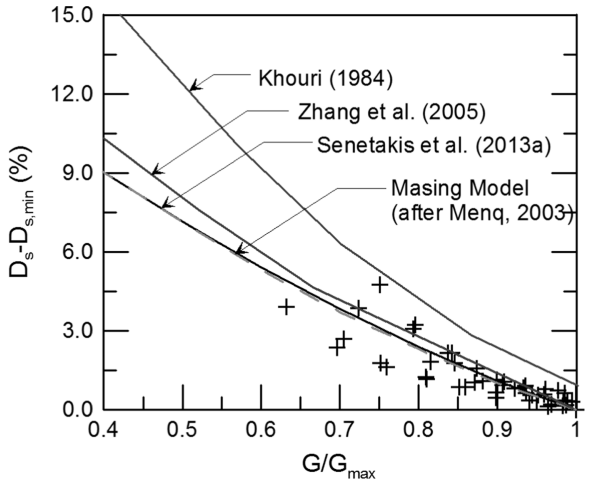

Fig. 18. Material damping, expressed as $D_s - D_{s,min}$, against the normalized shear modulus, G/G_{max}, for the RCA samples and corresponding curves proposed in the literature.

The difference in the a_s and a_p values for each fraction was, primarily, due to the differences in the initial density of the samples. In Fig. 13, representative plots of stiffness, by means of G_{max} against p' are given for the RCA04. In this figure, G_{max} is normalized with respect to a void ratio function proposed by Senetakis et al. (2012) in order to eliminate the effect of the void ratio on shear stiffness. This void ratio function is depicted in Fig. 13, where C_u is the coefficient of uniformity. The results indicated that at a given p', the normalized G_{max} values for all the samples, which had different initial densities, converged satisfactorily.

3.4. Poisson ratio during isotropic compression

Based on the measurement of shear and primary wave velocities from the bender and extender element tests, the dynamic Poisson's ratio for the fractions RCA04 and RCA05 was derived from Eq. (4). Because of the slightly higher sensitivity of V_s to pressure than the corresponding sensitivity of V_p, it is expected that the Poisson ratio will be pressure dependent.

Dynamic Poisson's ratio (ν) values against the isotropic confining pressure (p') for all the samples are summarized in Fig. 14. In agreement with previous studies on granular soils (e.g. Nakagawa et al., 1996; Kumar and Madhusudhan, 2010b; Wichtmann, Triantafyllidis Th., 2010), a slight decrease in the Poisson's ratio was observed with increasing confining pressure, with (ν) values that ranged from about 0.30 to 0.37 at $p' = 50$ kPa to values that ranged from 0.26 to 0.31 at $p' = 400$ kPa. These values are very similar with reported Poisson ratio on quartz sands by Wichtmann, Triantafyllidis Th. (2010). However, the results in Fig. 14 did not show a dependency between the Poisson's ratio and sample density or porosity. This is in agreement with the work by Wichtmann, Triantafyllidis Th. (2010), but in contrast with the slight trend of dependency of Poisson ratio on porosity reported by Kumar and Madhusudhan (2010b).

The ν–p' relationships were fitted with power law type curves of the general formula of Eq. (9):

$$\nu = a_\nu \times \left(p'\right)^{b_\nu} \tag{9}$$

The constants a_ν and b_ν for all the samples are summarized in Table 5. The constant a_ν ranged from 0.37 to 0.46 for the RCA04 and from 0.42 to 0.52 for the RCA05. The power b_ν was slightly greater, as an absolute value, for the fraction RCA05. Overall, the Poisson's ratio was slightly greater for the coarser RCA fraction (RCA05) at low pressures and the sensitivity of the Poisson's ratio to pressure was slightly greater for the RCA05 than the RCA04.

3.5. Comparison of small-strain stiffness of the RCA with literature models

A comparison of the small-strain shear modulus of the RCA samples with two models proposed in the literature by Senetakis et al. (2012) for river sand of relatively regular-shaped grains and crushed rock of irregular-shaped grains is given in Fig. 15. These two models are expressed through (Eqs. (10) and 11) for river sand and crushed rock, respectively. In these expressions, e denotes the void ratio at a given

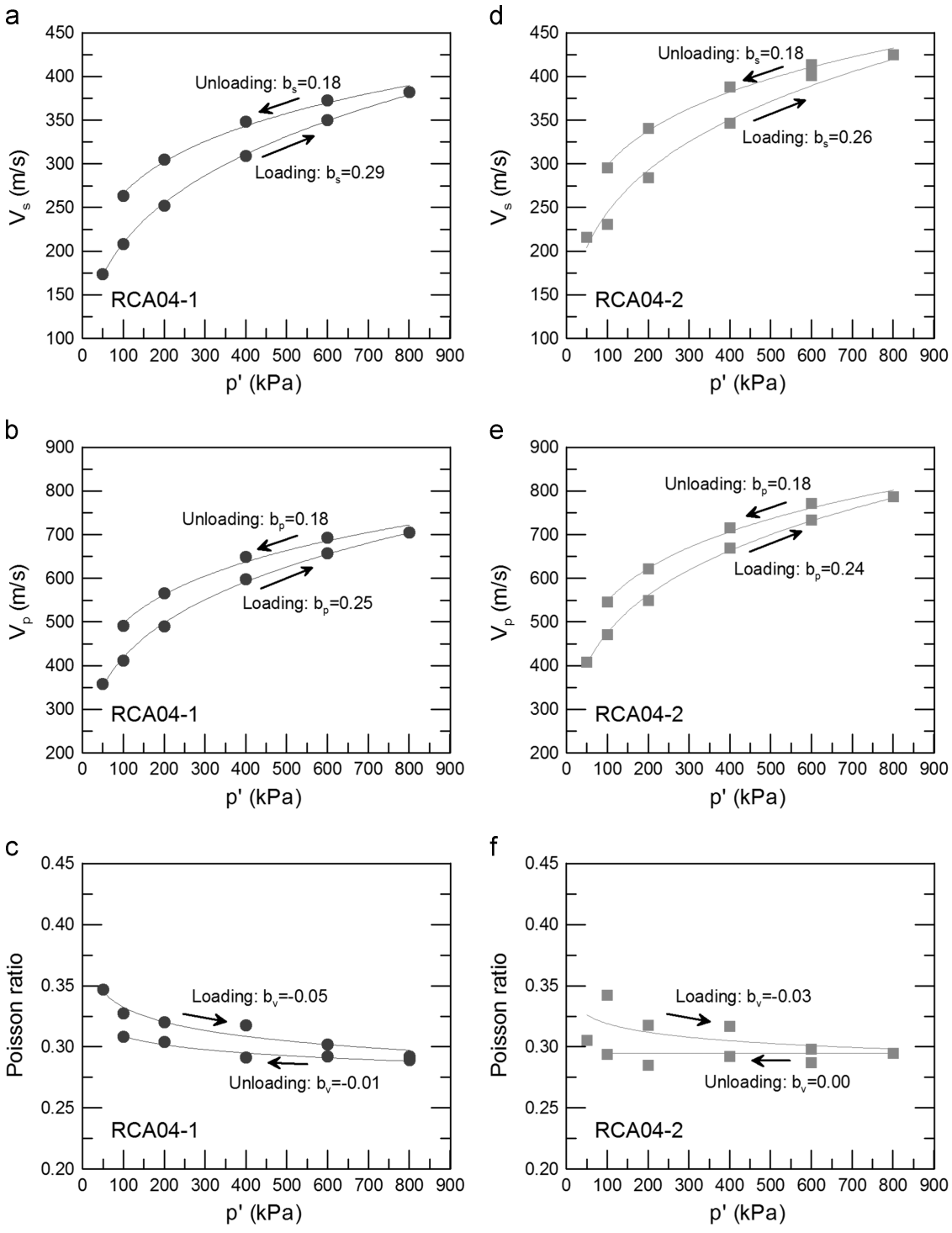

Fig. 19. Wave velocities and Poisson ratio during the isotropic compression and the isotropic swelling for the RCA04 samples (Note the important effect of mode of loading on the powers b_s, b_p and b_ν).

level of the confining pressure p', p_a denotes the atmospheric pressure and C_u denotes the coefficient of uniformity. Note that in (Eqs. (10) and 11), G_{max} is expressed in MPa. In order to use these expressions in the present study, for a given level of p', the corresponding void ratio derived from measurements of the axial strain and the assumption of isotropic compression of the samples, was used. Thus, the variables of these models are the void ratio and the confining pressure, whilst the coefficient of uniformity was kept constant for each sample, because for the range of pressures from 25 to 800 kPa used in the resonant column tests, no measurable change of the grading of the samples was observed, i.e. no significant

grain damage was observed.

$$G_{max} = (-5.88 \times C_u + 57.01) \times \left(\frac{1}{e^{0.28 \times C_u + 0.98}}\right) \times \left(\frac{p'}{p_a}\right)^{0.47} \quad (10)$$

$$G_{max} = (-9.45 \times C_u + 78.15) \times \left(\frac{1}{e^{0.28 \times C_u + 0.98}}\right) \times \left(\frac{p'}{p_a}\right)^{0.63} \quad (11)$$

The model derived on the basis of crushed rock provided an excellent prediction of the stiffness of the recycled concrete aggregate when the predicted shear modulus was plotted against the measured shear modulus. This excellent agreement can perhaps be attributed to the similarity of the grain shape of the samples of the present study and the study by Senetakis et al. (2012). Note that the satisfactory comparison between measured and estimated moduli in Fig. 15 should be considered as valid for the particular fractions of RCA (0.60–1.18 mm and 1.18–2.36 mm) and no general conclusions for different RCA fractions with different percentages of aggregate and cement mortar composition should be drawn before a thorough laboratory investigation is conducted.

3.6. Small-strain material damping and strain-dependent dynamic properties

Measurements of small-strain material damping ($D_{s,min}$) in torsional resonant column testing against p' were conducted on a small number of the RCA samples. Plots of $D_{s,min}$–p' are given in Fig. 16. Power-law type curves of the general formula of Eq. (12) were fitted to the experimental data. The values of the constants a_d and b_d are summarized in Fig. 16.

$$D_{s,min} = a_d \times \left(p'\right)^{b_d} \quad (12)$$

Material damping decreased slightly with an increase in the confining pressure, which is in agreement with the general trend observed in granular soils (Senetakis et al., 2012, 2013b, 2016; Senetakis and Madhusudhan, 2015). The power b_d was found relatively scattered with values that ranged from -0.07 to -0.27. This range of values is closer to reported values for sands of irregular-shaped grains (e.g. Senetakis et al., 2012; Senetakis and Madhusudhan, 2015). For the limited number of tests conducted in this study, $D_{s,min}$ was found slightly greater in magnitude than the reported values in the literature for quartz sands (Senetakis et al., 2012), crushed rock (Senetakis et al., 2012; Senetakis and Madhusudhan, 2015) and volcanic granular soils (Senetakis et al., 2013a, 2013b, 2016). Because of the scatter in the data (Senetakis et al., 2015), it should be noted that the correlation coefficient (r^2) between $D_{s,min}$ and p' is not as high as in the correlation between V_s and V_p with p'. For the wave velocities, r^2 was found equal to 0.99 or 1.00 for all the samples, whereas r^2 was found much lower in the case of damping. The r^2 values for the particular RCA samples are also depicted in Fig. 16.

For a set of four samples, medium-strain torsional resonant column tests were conducted at variable pressures (summarized in Table 4). Modulus degradation, normalized with respect to the small-strain value (G/G_{max}), and material damping increase (D_s) against the shear strain amplitude (γ) are plotted in Fig. 17. In the same figure, upper and lower bounds of non-linear curves proposed by Senetakis et al. (2013a) for quartz sands and crushed rock are plotted with a coefficient of uniformity of 1.4 and pressures of 100 kPa to 400 kPa figured into the literature expressions. The increase in the upper-lower bounds of modulus degradation and material damping proposed by Seed et al. (1986) for sands are also shown in Fig. 17. For the limited number of tests, the increase in stiffness degradation and material damping i for the RCA were plotted within the range proposed by Senetakis et al. (2013a). A slight dependency of the medium-strain normalized modulus and damping to pressure was observed. This trend is in agreement with the general trend observed in sands. In Fig. 17, a range of threshold strains reported by Senetakis et al. (2016) for granular soils is also shown. Senetakis et al. (2016) estimated the volumetric threshold, $\gamma_{t,v}$, on fully saturated granular soils as the shear strain amplitude beyond which significant pore water pressure buildup and thus, plastic deformations, occurred. On the other hand, the elastic threshold was computed as the shear strain for $G/G_{max} = 0.99$. Note that the experimental results by Senetakis et al. (2016) were based on torsional resonant column tests.

In Fig. 18, material damping, expressed as $D_s - D_{s,min}$, where $D_{s,min}$ is the small-strain damping, is plotted against the normalized shear modulus along with curves proposed in the literature (Khouri, 1984; Zhang et al., 2005; Masing model after Menq, 2003; Senetakis et al., 2013a). Within the scatter of the data, the values were plotted close to the literature curves, but in particular for G/G_{max} between 0.8 and 0.9, $D_s - D_{s,min}$ was plotted below the literature curves. While it may well be that the literature expressions provide an upper bound for material damping, further investigation is necessary for firm conclusions to be drawn. In modeling the non-linear response of geo-materials, a direct correlation of modulus degradation and material damping is convenient in particular when the data are used as input in computer codes that utilize the equivalent linear method for strong ground motion studies.

3.7. Behavior during isotropic swelling

Typical plots of V_s–p', V_p–p' and ν–p' for two samples of the RCA04 fraction during isotropic compression and isotropic swelling are given in Fig. 19. In the same figure, the power values b_s, b_p and b_ν during the isotropic loading and unloading stages are depicted. While V_s showed higher sensitivity to pressure than V_p, and the Poisson's ratio showed a clear pressure-dependency during isotropic compression, this was not observed systematically during the isotropic swelling of the samples. As shown in Fig. 19, during isotropic swelling, the power for shear and primary wave velocities was quite similar for each sample, which resulted in almost pressure-independent Poisson ratio. For all the samples in the study, the power b_ν for the Poisson's ratio had values in a range of -0.03 to -0.09 during isotropic compression, and values in a range of 0.00 to -0.03 during isotropic swelling.

In the literature, most studies associated with the elastic properties of granular soils have focused on small-strain shear modulus or shear wave velocities. Studies on the Young's modulus, primary wave velocities and the Poisson's ratio, based on laboratory test results, are relatively limited. While the pressure dependency of the Poisson's ratio in sands has been reported, this information is commonly associated with the behavior of sands during isotropic compression. The results of the study associated with the dynamic properties of recycled concrete aggregate may provide an excellent opportunity to study the behavior of granular soils since RCA is a granular material of relatively crushable grains. The slight dependency of the Poisson's ratio on pressure during the isotropic compression of the samples is in agreement with reported trends in the literature, but to the authors' knowledge, this is the first complementary work that reports the differences in the observed trends of the Poisson's ratio of the material during the loading (isotropic compression) and unloading (isotropic swelling) stages.

4. Conclusions

The dynamic properties of two uniform fractions of recycled concrete aggregate (RCA) were explored in this study. The geotechnical characterization of the RCA was based on conventional and simple laboratory tests and procedures. The specific gravity of solids was evaluated and the particle shape was quantified based on a visual observation of a representative number of grains and the use of an empirical chart. It was revealed that the RCA grains were shaped relatively irregularly. One-dimensional compression tests were carried out on dry samples and the grain damage was quantified using a simple method proposed in the literature. It was found that the breakage of the RCA grains for samples subjected to pressures from about 1.0 to 3.9 MPa was greater than the corresponding breakage in quartz sands, but lower than the breakage commonly found in highly crushable soils. CD monotonic triaxial tests were carried out on fully saturated samples of one fraction. An angle of shear strength at critical state of about 31 degrees was found. Values of the angle of shear strength at peak states and the corresponding states of the samples with respect to the critical were also reported.

Bender and extender element tests were conducted for the study of shear (V_s) and primary (V_p) wave velocities for the RCA. For V_s and V_p, average values derived from the first time arrival and the peak-to-peak time arrival methods were used. The V_s values from the bender element tests were quite similar to values derived from torsional resonant column tests using the same samples. Similarly, satisfactory agreement was found between Young's moduli derived directly from flexural resonant column tests and indirectly from the extender element tests. During the isotropic compression of the samples, V_s showed higher sensitivity to pressure than V_p, and the Poisson's ratio showed a clear dependency on pressure. Fitting curves of a power law type were used to estimate the elastic constants of the samples. During the isotropic swelling of the samples, V_s and V_p showed similar sensitivity to pressure and interestingly, the Poisson's ratio was found almost independent to pressure.

Measurements of small-strain materials damping for a limited number of tests showed values of $D_{s,min}$ slightly higher than values reported in the literature for dry sand. The sensitivity of $D_{s,min}$ to pressure was similar to that reported in the literature for crushed sand. Finally, medium-strain resonant column tests were performed for a representative number of samples. The strain-dependent modulus and damping were found within the upper-lower bounds of non-linear curves proposed in the literature for sands. In capturing the complete behavior of geomaterials, the knowledge of modulus, damping and Poisson ratio is important. The results of this study showed that for crushable soils, the behavior during isotropic swelling should not be ignored in laboratory research works because the elastic properties of soils may have a different sensitivity to pressure depending on whether the soil is under isotropic compression or isotropic swelling.

Acknowledgments

The authors would like to acknowledge the anonymous reviewers for their constructive comments that helped us to improve the quality of the manuscript. During this study, the first author is supported from a scholarship funded by the Faculty of Engineering UNSW and the School of Civil and Environmental Engineering UNSW and the second author is supported partly by a Faculty Research Grant (FRG, PS38513). The Technical Officers Mr Paul Gwynne and Mr Timothy Weston are acknowledged for their patience and continuous support during the development and setup of the laboratory facilities. Miss Irene Calaizis, Manager of the CIES, and Miss Patricia Karwan, Administrative Officer, are also acknowledged for their continuous assistance in the efficient management of the FRG project and Professor Stephen Foster (Head of School) is acknowledged for his generous financial support in the development of the new soil dynamics laboratory facilities of UNSW.

References

Altuhafi, F.N., Coop, M.R., 2011. Changes to particle characteristics associated with the compression of sands. Geotechnique 61 (6), 459–471.

Arulrajah, A., Piratheepan, J., Disfani, M.M., Bo, M.W., 2013. Geotechnical and geoenvironmental properties of recycled construction and demolition materials in pavement subbase applications. J. Mater. Civil. Eng. 25 (8), 1077–1088.

ASTM, 1992. Standard test methods for modulus and damping of soils by the resonant column method: D4015-92, Annual Book of ASTM Standards. ASTM International.

Been, K., Jefferies, M.G., 1985. A state parameter for sands. Geotechnique 35 (2), 99–112.

Bhuiyan, M.Z.I., Ali, F.Hj, Salman, F.A., 2015. Applications of recycled concrete aggregates as alternative granular infills in hollow segmental block systems. Soils Found. 55 (2), 296–303.

Cascante, G., Santamarina, C., Yassir, N., 1998. Flexural excitation in a standard torsional-resonant column. Can. Geotech. J. 35, 478–490.

Cha, M.C., Santamarina, J.C., Kim, H.-S., Cho, G.-C., 2014. Small-strain stiffness, shear-wave velocity, and soil compressibility. J. Geotech. Geoenviron. Eng. 140 (10), 06014011.

Chini, A.R., Kuo, S.S., Armaghani, J.M., Duxbury, J.P., 2001. Test of recycled concrete aggregate in accelerated test track. J. Transp. Eng. 127 (6), 486–492.

Cho, G.-C., Dodds, J., Santamarina, C., 2006. Particle shape on packing density, stiffness, and strengt. J. Geotech. Geoenviron. Eng. 132, 591–602.

Ghafghazi, M., Shuttle, D.A., DeJong, J.T., 2014. Particle breakage and the critical state of sand. Soils Found. 54 (3), 451–461.

Gomes Correia, A., Roque, A.J., Reis Ferreira, S.M., Fortunato, E., 2012. Case study to promote the use of industrial byproducts: the relevance of performance tests. J. ASTM Int. 9 (2) http://dx.doi.org/10.1052/JAI103705.

Gu, X., Yang, J., Huang, M., Gao, G., 2015. Bender element tests in dry and saturated sand: Signal interpretation and result comparison Available online. Soils Found. 55 (5), 951–962.

Hardin, B., Richart, F., 1963. Elastic wave velocities in granural soils. J. Soil Mech. Found. 89, 33–65.

Hardin, B.O., 1985. Crushing of soil particles. J. Geotech. Eng. 111 (10), 1177–1192.

Ishihara, K., 1996. Soil behaviour in earthquake geotechnics. Oxford Science Publications.

Jovicic, V., Coop, M.R., Simic, M., 1996. Objective criteria for determining G_{max} from bender element tests. Geotechnique 46 (2), 357–362.

Khouri N. 1984. Dynamic properties of soils. M.S. Dissertation, Department of Civil Engineering, Syracuse University.

Krumbein, W., Sloss, L., 1963. Stratigraphy and sedimentation. W.H. Freeman and Company, San Francisco.

Kumar, J., Madhusudhan, B.N., 2010a. On determining the elastic modulus of a cylindrical sample subjected to flexural excitation in a resonant column apparatus. Can. Geotech. J. 47, 1288–1298.

Kumar, J., Madhusudhan, B.N., 2010b. Effect of relative density and confining pressure on Poisson ratio from bender and extender elements tests. Geotechnique 60 (7), 561–567.

Kumar, J., Madhusudhan, B.N., 2010c. A note on the measurement of travel times using bender and extender elements. Soil. Dyn. Earthq. Eng. 30, 630–634.

Lee, J.-S., Santamarina, J.C., 2005. Bender elements: performance and signal interpretation. J. Geotech. Geoenviron. Eng. 131 (9), 1063–1070.

Leong, E.C., Yeo, S.H., Rahardjo, H., 2005. Measuring shear wave velocity using bender elements. Geotech. Test. J. 28 (5), 1–11.

Leong, E.C., Cahyadi, J., Rahardjo, H., 2009. Measuring shear and compression wave velocities of soils using bender-extender elements. Can. Geotech. J. 46, 792–812.

Menq, F.-Y., 2003. Dynamic Properties of Sandy and Gravelly Soils Ph. D. Dissertation. University of Texas at Austin, USA.

Nakagawa, K., Soga, K., Mitchell, J.K., 1996. Pulse transmission system for measuring wave propagation in soils. J. Geotech. Eng. 122, 302–308.

Nakata, Y., Hyodo, M., Hyde, A.F.L., Kato, Y., Murata, H., 2001. Microscopic particle crushing of sand subjected to high pressure one-dimensional compression. Soils Found. 41 (1), 69–82.

Ogino, T., Kawaguchi, T., Yamashita, S., Kawajiri, S., 2015. Measurement deviations for shear wave velocity of bender element test using time domain, cross-correlation, and frequency domain approaches. Soils Found. 55 (2), 3229–3342.

Payan, M., Khoshghalb, A., Senetakis, K., Khalili, N., 2016. Effect of particle shape and validity of G_{max} models for sand: a critical review and a new model. Comput. Geotech. 72, 28–41.

Poon, C.S., Chan, D., 2006a. Paving blocks made with recycled concrete aggregate and crushed clay brick. Constr. Build. Mater. 20, 569–577.

Poon, C.S., Chan, D., 2006b. Feasible use of recycled concrete aggregates and crushed clay brick as unbound road sub-base. Constr. Build. Mater. 20, 578–585.

Richart, F.E., Hall, J.R., Woods, R.D., 1970. Vibrations of soils and foundations. Prentice Hall, Englewood Cliffs, 414.

Rocchi, I., Coop, M.R., 2014. Experimental accuracy of the initial specific volume. Geotech. Test. J. 37 (1), 169–175.

Santamarina, C., Cascante, G., 1998. Effect of surface roughness on wave propagation parameters. Geotechnique 48 (1), 129–136.

Seed, H., Wong, R., Idriss, I., Tokimatsu, K., 1986. Moduli and damping factors for dynamic analysis of cohesionless soils. J. Geotech. Eng. 112, 1016–1103.

Senetakis, K., Anastasiadis, A., Pitilakis, K., 2012. The small-strain shear modulus and damping ratio of quartz and volcanic sands. Geotech. Test. J. 35 (6) http://dx.doi.org/10.1520/GTJ20120073.

Senetakis, K., Anastasiadis, A., Pitilakis, K., 2013a. Normalized shear modulus reduction and damping ratio curves of quartz sand and rhyolitic crushed rock. Soils Found. 53 (6), 879–893.

Senetakis, K., Anastasiadis, A., Pitilakis, K., Coop, M., 2013b. The dynamics of a pumice granular soil in dry state under isotropic resonant column testing. Soil. Dyn. Earthq. Eng. 45, 70–79.

Senetakis, K., Madhusudhan, B.N., 2015. Dynamics of potential fill-backfill material at very small strains. Soils Found. 55 (5), 1196–1210.

Senetakis, K., Anastasiadis, A., Pitilakis, K., 2015. A comparison of material damping measurements in resonant column using the steady-state and free-vibration decay methods. Soil. Dyn. Earthq. Eng. 74, 10–13.

Senetakis, K., Madhusudhan, B.N., Anastasiadis, A., 2016. Wave propagation attenuation and threshold strains of fully saturated soils with intra-particle voids. J. Mater. Civil Eng. 28, 04015108.

Shipton, B., Coop, M.R., 2012. On the compression behaviour of reconstituted soils. Soils Found. 52 (4), 668–681.

Shirley, D., Anderson, A., 1975. In situ measurement of marine sediment acoustical properties during coring in deep water. IEEE Trans. Geosci. Electron. GE-13, 163–169.

Sivakumar, V., McKinley, J.D., Ferguson, D., 2004. Reuse of construction waste: performance under repeated loading. Proc. Inst. Civil. Eng.: Geotech. Eng. 157 (2), 91–96.

Soleimanbeigi, A., Edil, T.B., Benson, C.H., 2012. Recycled asphalt shingles mixed with granular byproducts as structural fills. J. ASTM Int. 9 (1) http://dx.doi.org/10.1520/JAI103766.

Tam, V.W.Y., Tam, C.M., 2007. Crushed aggregate production from centralized combined and individual waste sources in Hong Kong. Constr. Build. Mater. 21 (4), 879–886.

Vilhar, G., Jovicic, V., Coop, M.R., 2013. The role of particle breakage in the mechanics of a non-plastic silty sand. Soils Found. 53 (1), 91–104.

Warner, J.D., Edil, T.B., 2012. An evaluation of reclaimed asphalt shingles for beneficial reuse in roadway construction. J. ASTM Int. 9 (1) http://dx.doi.org/10.1520/JAI103665.

Wichtmann, T., Triantafyllidis Th, 2009. Influence of the grain-size distribution curve of quartz sand on the small strain shear modulus G_{max}. J. Geotech. Geoenviron. Eng. 135, 1404–1418.

Wichtmann, T., Triantafyllidis Th, 2010. On the influence of the grain size distribution curve on P-wave velocity, constrained modulus M_{max} and Poisson's ratio of quartz sand. Soil. Dyn. Earthq. Eng. 30, 757–766.

Zhang, J., Andrus, R., Juang, C., 2005. Normalized shear modulus and material damping ratio relationships. J. Geotech. Geoenviron. Eng. 131, 453–464.